AGU ADVANCING EARTH AND SPACE SCIENCES

Geophysical Research Letters

RESEARCH LETTER
10.1029/2025GL115334

The Global Influence of ENSO on Rapid Intensification of Tropical Cyclones

L. G. Silvers[1], P. J. Klotzbach[1], C. J. T. Allen[2], M. M. Bell[1], S. G. Bowen[3], S. S. Chand[4], M. Ekström[2], M. Hemmati[5,6], and C. J. Schreck III[7]

[1]Department of Atmospheric Science, Colorado State University, Fort Collins, CO, USA, [2]Gallagher Re, London, UK, [3]Gallagher Re, Chicago, IL, USA, [4]Institute of Innovation, Science and Sustainability, Federation University, Ballarat, VIC, Australia, [5]Gallagher Re, New York, NY, USA, [6]Lamont-Doherty Earth Observatory, Columbia University, New York, NY, USA, [7]North Carolina Institute for Climate Studies, Cooperative Institute for Satellite Earth Systems Studies, North Carolina State University, Asheville, NC, USA

Abstract Tropical cyclone (TC) rapid intensification (RI) is a major source of uncertainty in TC prediction. Here we examine observed basin-specific relationships between RI and El Niño-Southern Oscillation (ENSO), where RI is defined as a TC strengthening by ≥30 kt within 24 hr. During El Niño, the number of RI events significantly increases in the eastern North Pacific, western North Pacific and South Pacific, with the opposite behavior in the North Atlantic. During La Niña, changes in RI occurrence in the Atlantic and Pacific are approximately opposite as in El Niño. The ENSO–Indian Ocean RI relationship is weak. These changes are consistent with environmental conditions modulating RI, including mid-level moisture, vertical wind shear, sea surface temperatures and potential intensity. Because of disagreement between the recently observed La Nina-like trend and an El Niño-like trend simulated by climate models, improved model representation of ENSO could reduce future uncertainty in RI projections.

Plain Language Summary El Niño-Southern Oscillation (ENSO) modulates both global tropical cyclone activity and the rapid intensification of tropical cyclones. Here we focus on rapidly intensifying tropical cyclones (defined to be storms intensifying by ≥30 kt in a 24-hr period) because these storms historically have been more challenging to predict and often are responsible for major damage when they make landfall. For example, over 80% of North Atlantic hurricanes since 1980 that made landfall in the United States (causing >$5 billion US dollars in damage) underwent rapid intensification at some point during their lifetime. These modulations in rapidly intensifying tropical cyclones are linked to environmental conditions, with RI likelihood increasing with increased mid-level moisture, reduced vertical wind shear (the change in wind speed and direction with height), and increased sea surface temperatures. Here, we examine the observed relationship between ENSO and global rapid intensification of tropical cyclones. El Niño, the positive phase of ENSO, significantly increases rapid intensification in the eastern North Pacific, western North Pacific and South Pacific basins, while La Niña shows an approximately opposite relationship, with increased rapid intensification in the North Atlantic. An improved understanding of future ENSO trends is critical for better anticipating future trends in rapid intensification.

L. G. Silvers and P. J. Klotzbach contributed equally to this work.

Key Points:

- Frequency of rapid intensification differs considerably for individual tropical cyclone basins and different ENSO phases
- Atlantic rapid intensification occurs more frequently in La Niña and less frequently in El Niño, with opposite relationship in Pacific
- Future ENSO trend uncertainty implies ambiguity in projections of future basin and global-scale rapid intensification

Supporting Information:

Supporting Information may be found in the online version of this article.

Correspondence to:

L. G. Silvers,
levi.silvers@colostate.edu

Citation:

Silvers, L. G., Klotzbach, P. J., Allen, C. J. T., Bell, M. M., Bowen, S. G., Chand, S. S., et al. (2025). The global influence of ENSO on rapid intensification of tropical cyclones. *Geophysical Research Letters*, *52*, e2025GL115334. https://doi.org/10.1029/2025GL115334

Received 13 FEB 2025
Accepted 19 SEP 2025

1. Introduction

Rapid intensification (RI) of tropical cyclones (TCs) occurs when a TC intensifies quickly and is often calculated over a 24-hr period. Typically, a definition of ≥30 kt 24 hr^{-1} has been taken to define RI (Kaplan & DeMaria, 2003), corresponding to approximately the 95th percentile of overwater intensification rates for TCs. An improved understanding of RI is critical due to the impactful nature of these storms. For example, Majumdar et al. (2023) found that 25 out of 30 North Atlantic hurricanes making landfall in the US underwent RI. These 30 hurricanes caused >$5 billion (USD) in Consumer Price Index (CPI)-adjusted damage from 1980 to 2021.

Prior research has shown that RI is a product of both favorable large-scale environmental conditions (e.g., Hendricks et al., 2010; Majumdar et al., 2023; Richardson et al., 2022; Rozoff & Kossin, 2011) and a conducive inner core (e.g., DesRosiers et al., 2023; Hazleton et al., 2020; Miyamoto & Nolan, 2018). Specifically, anomalously warm sea surface temperatures (SSTs), increased potential intensity (PI), high mid-level relative humidity (RH), low vertical wind shear and enhanced vertical motion all promote RI (Rozoff & Kossin, 2011). Inner core characteristics favoring RI include taller TC vortices (DesRosiers et al., 2023) and TCs with a small and

contracting radius of maximum winds (Majumdar et al., 2023; Stern et al., 2015). There have been numerous other recent studies that investigated various characteristics of RI (e.g., Bhatia et al., 2019, 2022; Cha et al., 2020; Y. Guo & Tan, 2021; Klotzbach, 2012; Li et al., 2023; Ng & Vecchi, 2020; Trabing & Bell, 2020; Wang et al., 2017). This study focuses on climatological and interannual modulations of RI likely driven by fluctuations of environmental conditions as modulated by El Niño-Southern Oscillation (ENSO; Rasmusson & Carpenter, 1982).

ENSO is the leading driver of interannual tropical climate variability with demonstrated impacts on TC activity for various ocean basins, including the North Atlantic (NA; Klotzbach, 2011; Mueller et al., 2024), eastern North Pacific (ENP; Balaguru et al., 2020; Collins et al., 2016), western North Pacific (WNP; Patricola et al., 2018; Zhao et al., 2023), North Indian (NI; Das et al., 2023; Roose et al., 2022), South Indian (SI; Astier et al., 2015; Ho et al., 2006), Australian (Chand et al., 2013; Dowdy, 2014) and South Pacific (SP; Magee et al., 2020). These are just a few examples of papers that have noted the ENSO-TC relationship in each basin. We recommend Lin et al. (2020) for a thorough literature review. The most important drivers of the ENSO-TC relationship vary from basin-to-basin (Camargo et al., 2007; Lin et al., 2020), but involve both dynamic and thermodynamic variables including SSTs, mid-level relative RH, low-level vorticity, and vertical wind shear.

While considerable research has focused on relationships between ENSO and TC activity in individual basins, fewer studies have looked at the interannual relationship between ENSO and TC activity on a global scale (Camargo et al., 2007; Lin et al., 2020; Patricola et al., 2022). These studies have either focused on individual storms, or storm statistics including the number of TCs, hurricanes (e.g., maximum sustained winds ≥64 kt), and Accumulated Cyclone Energy. To our knowledge, no study has comprehensively documented how ENSO modulates the global frequency and distribution of TCs that undergo RI.

To fill this gap, we examine how ENSO modulates RI globally using data from 1990 to 2023 (e.g., Figure 2), a period that is considered to have high-quality TC track information (Klotzbach & Landsea, 2015). Because of the known impact of the large-scale tropical environment on TCs and RI, we also investigate ENSO in a selection of CMIP6 climate models, noting the disagreement in the recently observed La Niña-like trend and the model-projected El Niño-like future trend (e.g., Lee et al., 2022; Sobel et al., 2023; Watanabe et al., 2024).

2. Data

2.1. Tropical Cyclone Data Set

We utilize US warning agency data from 1990 to 2023 from the International Best Track Archive for Climate Stewardship version 4 (IBTrACSv4; Knapp et al., 2010) for all TC basins. This includes the National Hurricane Center archive, HURDAT2 (Landsea & Franklin, 2013), for the NA and ENP basins and the Joint Typhoon Warning Center archive (Chu et al., 2002) for all other basins. US warning agency data were used due to a consistent wind averaging time (e.g., one-minute maximum sustained wind) for all TC basins, although there are some slight differences between these data sets and the World Meteorological Organization agency data sets (e.g., Kumar et al., 2025; Schreck et al., 2014). The ENP and WNP basins are separated at the International Date Line, while the SI and SP basins are separated at 135°E, as in Klotzbach et al. (2022).

2.2. Environmental Parameter Data Set

We use monthly data from the 5th generation reanalysis from the European Centre for Medium-Range Weather Forecasts (ERA5; Hersbach et al., 2020) at a 0.25° spatial resolution for observationally derived large-scale data from 1990 to 2023. Here we analyze the following variables: relative SST (Vecchi & Soden, 2007), 700 hPa RH, 200 minus 850 hPa vertical wind shear and potential intensity (Bister & Emanuel, 2002). Relative SST (hereafter rSST) was calculated by subtracting the monthly tropical mean (30°S–30°N) from the local SST at each grid point. Potential intensity (PI) was calculated using the pyPI algorithm of Gilford (2020, 2021), with details provided in Text S1 of Supporting Information S1. These four parameters are closely tied to the environmental favorability for TC formation and intensification (e.g., Camargo et al., 2007; Majumdar et al., 2023; Ramsay & Sobel, 2011). The PI is a composite metric that incorporates thermodynamic constraints and environmental conditions to derive an upper limit of the intensity of tropical cyclones (Emanuel, 1986).

10.1029/2025GL115334

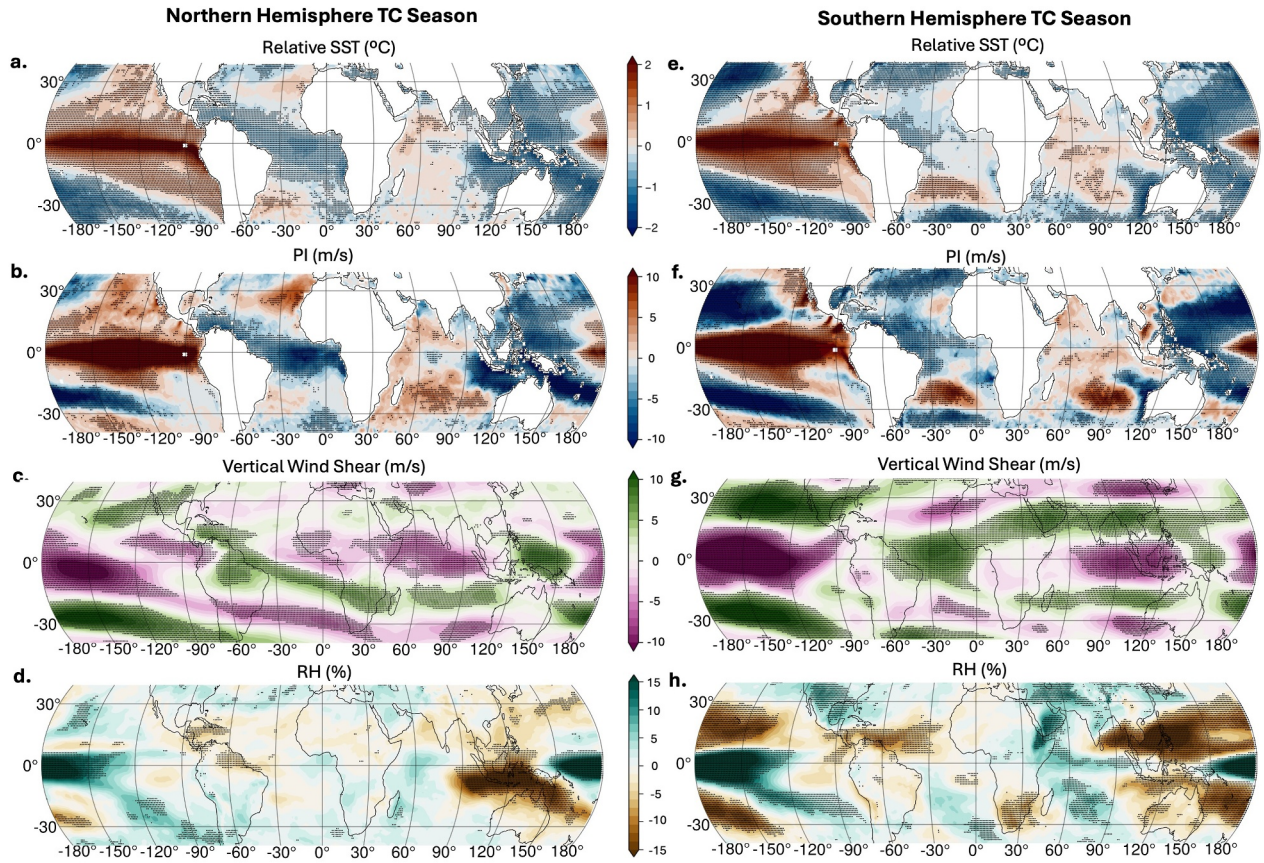

Figure 1. Large-scale composite environmental conditions (El Niño years minus La Niña years). The left column (a–d) shows the Northern Hemisphere TC season (June–November), while the right column (e–h) shows the Southern Hemisphere TC season (November–April). (a, e) rSST difference (°C), (b, f) PI difference (m s^{-1}), (c, g) 200–850-hPa vertical wind shear difference (m s^{-1}), and (d, h) 700 hPa RH difference (%). Black circles indicate grid points with statistical significance at the 0.05 level after controlling for the false discovery rate (Wilks, 2016).

2.3. Climate Model Data Set

To explore future trends in ENSO, we use data from 20 global climate models (GCMs) that participated in the Coupled Model Intercomparison Project phase 6 (CMIP6; Eyring et al., 2016). Details of the GCMs are provided in Text S2 and Table S1 of Supporting Information S1. We used data from the *historical* and the Shared Socioeconomic Pathway *SSP5-8.5* simulations. The *historical* simulations are global, fully coupled simulations between 1850 and 2014, forced by the observed aerosols, concentrations of atmospheric greenhouse gases, and land use. The *SSP5-8.5* represents a high-emission scenario that assumes future fossil-fuel development and a growing economy with additional radiative forcing of 8.5 Wm^{-2} by the year 2100 (O'Neill et al., 2016). Because these models operate at a relatively coarse resolution (~100 km), they under-resolve many important characteristics of TCs (Roberts et al., 2020). Given these limitations, our analysis focuses on projected changes in ENSO based on an analysis of SST. We infer some implications for future TC RI based on these simulations.

3. Methods

3.1. Rapid Intensification Classification

TC intensity changes are calculated over a 24-hr period using observations occurring at 0 UTC, 6 UTC, 12 UTC and 18 UTC. We analyze both individual RI events and RI storms. An RI storm is defined as a system of at least tropical storm strength (≥34 kt) that undergoes one or more 30+ kt 24 hr^{-1} intensification events (Klotzbach et al., 2022). We exclude RI events that began at tropical depression strength due to the less reliable classification of tropical depressions (Klotzbach & Landsea, 2015). Both RI storms and RI events are calculated at two thresholds: 30+ kt 24 hr^{-1} and 50+ kt 24 hr^{-1}. If a system underwent RI for multiple consecutive 24-hr periods

(e.g., 0 UTC 25 September to 0 UTC 26 September and 6 UTC 25 September to 6 UTC 26 September), then multiple RI events are counted.

We examine RI during June–November for the Northern Hemisphere and November–April for the Southern Hemisphere. These months encompass 90% of all RI events for the Northern Hemisphere and 98% of all RI events for the Southern Hemisphere during 1990–2023. Our analysis extends from June 1990 to November 2023 for the Northern Hemisphere and from November 1989 to April 2023 for the Southern Hemisphere. In the Southern Hemisphere, a TC season is labeled with the second year, so the November 1989–April 1990 TC season is referred to as the 1990 TC season.

3.2. ENSO Classification

The Relative Oceanic Nino Index (RONI; van Oldenborgh et al., 2021; L'Heureux et al., 2024) is a recently defined ENSO metric that highlights the spatial temperature variations of the Niño 3.4 SST index (5°S–5°N, 170–120°W) after subtracting the mean tropical SST. We employ the RONI index to classify ENSO events and thus reduce a potential bias from the mean trend of tropical SST. Following L'Heureux et al. (2024), we use the Extended Reconstructed SST version 5 (Huang et al., 2017) to calculate the RONI (see Text S3 in Supporting Information S1 for details on the calculation method). The 8 years with the warmest RONI values (approximately the upper quartile) during June–November (November–April) are classified as El Niño for the Northern (Southern) Hemisphere, and the 8 years with the coldest RONI values (approximately the lower quartile) during June–November (November–April) are classified as La Niña for the Northern (Southern) Hemisphere. All other years are classified as neutral. Using this definition, 0.60°C (−0.82°C) is used for the El Niño (La Niña) threshold in June–November, while 0.43°C (−0.79°C) is used as the El Niño (La Niña) threshold in November–April. All years selected have the same convention as for TC classification (e.g., November 1989–April 1990 is referred to as 1990 for the Southern Hemisphere). Table S2 in Supporting Information S1 displays El Niño/La Niña years based on this classification methodology.

3.3. Statistical Significance Tests

Significance of composite environmental fields was tested with a two-tailed one sample *t*-test at the 0.05 level at each grid point. To account for the expected false discovery rate we used the method described in Wilks (2016). For basin-wide statistics use a permutation test without replacement repeated 1,000 times (Good, 2005) to test for statistical significances of means at the 10% level. We evaluate how the means of various RI statistics for El Niño, La Niña and neutral ENSO years compare with the mean of the full 34-year period. If the mean of the observed rate for a particular ENSO phase is less than the 50th or greater than the 950th value of the randomly resampled values from the full 34-year sample (e.g., 8 years for El Niño/La Niña and 18 years for ENSO neutral), it is deemed to be statistically significant at the 10% level using a two-tailed test. Statistical significance for the event density plot was calculated using a chi-square test at the 10% level.

4. Results

4.1. Large-Scale Environmental Conditions

El Niño minus La Niña composite fields for several large-scale environmental conditions during the Northern Hemisphere and Southern Hemisphere peak TCs seasons are displayed in Figure 1. We display the full tropical circulation for both the Northern and Southern Hemisphere peak TC season to highlight how ENSO's modulations of environmental conditions change from the boreal to the austral summer and fall.

El Niño minus La Niña differences in the Northern Hemisphere and Southern Hemisphere peak TC seasons are quite similar, as was found in Camargo et al. (2007). As shown in Vecchi and Soden (2007), rSST (Figures 1a and 1e) can serve as an excellent proxy for the PI (Figures 1b and 1f).

By definition, rSSTs are significantly warmer in El Niño than La Niña across most of the eastern and central tropical Pacific (Figures 1a and 1e). In the western part of the WNP, rSSTs are significantly cooler in El Niño as the western Pacific warm pool discharges its heat eastward (e.g., Jin, 1997). While the rSST warming is maximized along the equator, there are also significantly positive rSST anomalies extending to ∼15°N, which combined with increased mid-level RH (Figures 1d and 1h), creates a more favorable thermodynamic environment for TCs across most of the ENP. El Niño-driven vertical wind shear changes in the ENP also broadly favor RI, with

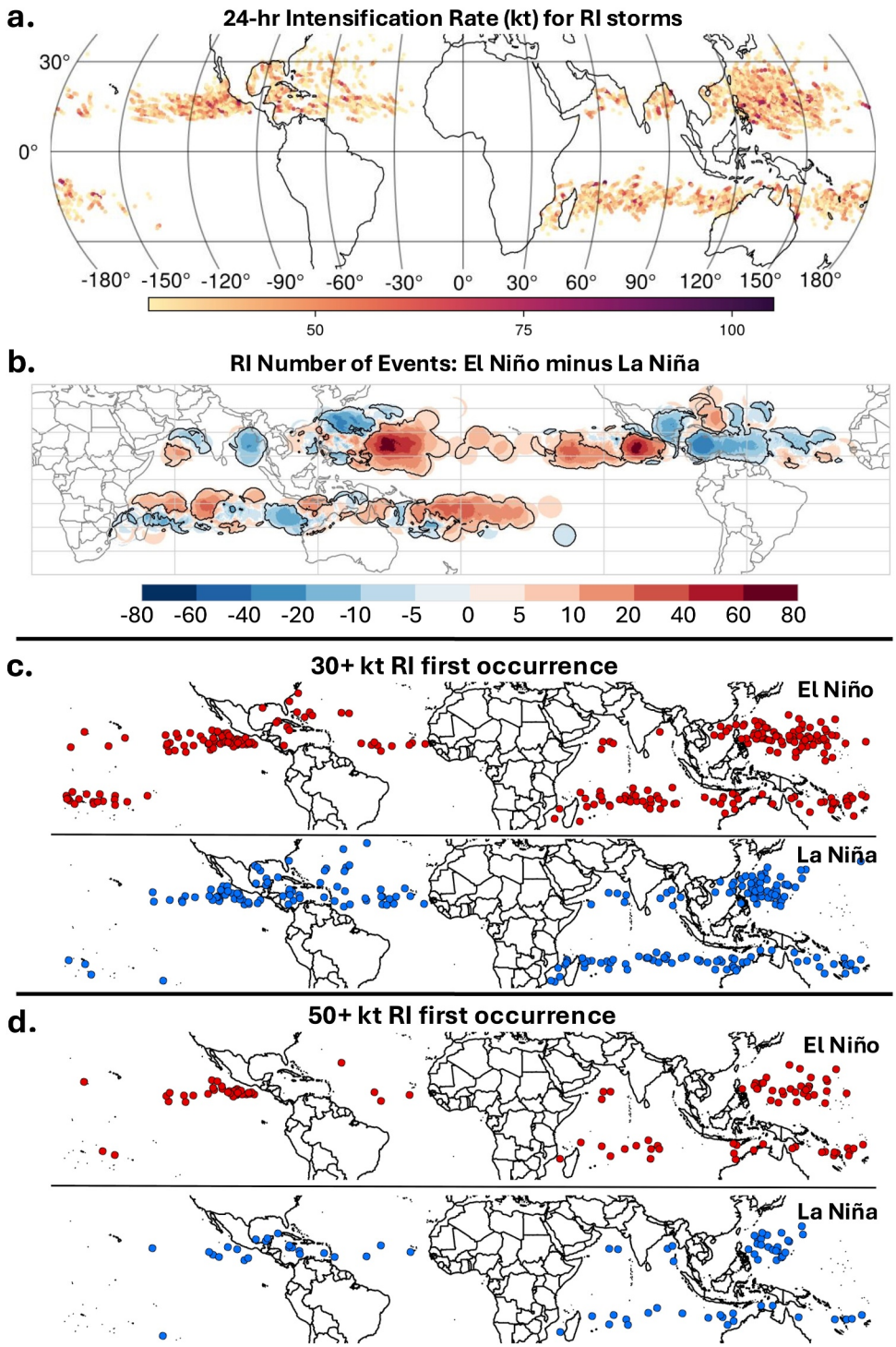

Figure 2. Geography of RI. (a) 24-hr intensification rate (kt) for all 30+ kt RI events during our study period (1990–2023). (b) 30+ kt RI composite event density for El Niño minus La Niña. The black contour in (b) denotes statistical significance at the 10% level. (c) Location where TCs first underwent 30+ kt RI during El Niño (red) and La Niña (blue). Panel (d) as in panel (c) but for locations where TCs first underwent 50+ kt RI.

significantly reduced shear across most of the basin. In the eastern WNP basin, significantly reduced shear, warmer rSSTs and increased mid-level RH and PI create TC favorable conditions, while significantly increased shear, cooler rSSTs and decreased mid-level RH and PI disfavor TC activity in the western part of the WNP basin.

In the NA, El Niño significantly increases vertical wind shear in the western part of the basin and reduces RH relative to La Niña, making for unfavorable TC conditions (Figures 1c and 1d). El Niño's suppressing influence in the Atlantic via increases in vertical wind shear has been documented in many prior studies (e.g., Lin et al., 2020). These El Niño-driven differences are close to the inverse of the correlation between NA 30+ kt 24 hr^{-1} number and global rSST, PI, vertical wind shear and RH (Figure S1 in Supporting Information S1).

In the NI, environmental conditions are mixed, with reduced shear favoring RI but decreased RH and rSSTs/PI disfavoring RI (Figures 1a–1d). While the SIO generally has increased vertical wind shear in El Niño relative to La Niña (Figure 1g), the thermodynamic environment to the east of Madagascar is somewhat more conducive for TCs, with significantly increased rSSTs, PI, and mid-level RH (Figures 1e, 1f and 1h). Near Australia, environmental conditions are less favorable for TCs in El Niño, with significantly reduced rSSTs and PI, decreased mid-level RH and increased vertical wind shear (Figures 1e–1h). Farther east in the SP, warmer rSSTs, increased mid-level RH and PI and decreased vertical wind shear favor TC activity in El Niño.

4.2. Regional Differences in RI by ENSO Phase

RI events occur in all TC basins (Figure 2a). Regions with higher concentrations (Figure 2c) include west of Mexico and near the Philippines in the WNP. In the NA, RI events are most frequent in the Caribbean and Gulf of Mexico, where SSTs are climatologically the warmest. RI numbers are largely uniform across the Southern Hemisphere from Mozambique to the International Date Line. While SSTs can be extremely warm and PI large in the central Pacific, this region tends to experience a pronounced tropical upper tropospheric trough which increases vertical wind shear and promotes dry air advection, reducing both overall TC frequency and RI occurrence (Wang et al., 2020).

To visualize the relationship between RI and ENSO phase, we use an event density map (Figure 2b) and maps of the location where TCs first undergo RI (Figures 2c and 2d). While the general pattern of dependence on ENSO phase is consistent regardless of RI threshold, the signal is generally clearer for the cases of 50+ kt RI (Figure 2d). During La Niña seasons, the western Atlantic becomes much more favorable for 50+ kt RI TCs. In contrast, no 50+kt RI TCs have occurred in El Niño seasons west of 60°W (Figure 2d). This increase in RI TCs in the NA during La Niña is primarily due to reductions in vertical wind shear that occur during La Niña (Klotzbach, 2011). El Niño increases ENP 50+ kt RI TCs west of Mexico and increases their chances of formation in the central portion of the North Pacific. The ENP becomes more favorable thermodynamically during El Niño (Figure 1), as has also been noted by Collins et al. (2016) and Balaguru et al. (2020). During El Niño, a pronounced southeastward shift in RI TCs occurs in the WNP (Figures 2b–2d) due to increases in SST and PI, tropospheric RH and decreases in vertical wind shear during El Niño years (Figure 1). The sample size of 50+ kt RI TCs is small in the NI. However, we note there have been no 50+ kt RI TCs in the Bay of Bengal during El Niño years.

We do not observe any pronounced spatial shifts or frequency differences in SI 50+ kt RI TCs (Figure 2d). In the SP, however, we find more 50+ kt RI TCs east of Australia in El Niño, due to a more TC-favorable South Pacific Intertropical Convergence Zone and increased mid-level RH (Camargo et al., 2007).

4.3. Basinwide Differences in RI by ENSO Phase

Globally, we find that more storms undergo RI during El Niño than La Niña. The Northern Hemisphere averages nine 50+ kt RI storms in El Niño and six 50+ kt RI storms in La Niña—a statistically significant increase. The difference in the Southern Hemisphere is not significant (four 50+ kt RI storms in El Niño and three 50+ kt RI storms in La Niña). This reflects the higher storm counts and larger geographic region of the Pacific basin relative to the Atlantic basin.

An opposite relationship between the NA and the ENP for several different TC metrics was noted in Patricola et al. (2022). Here we note a similar opposite relationship for RI activity. The ENP shows statistically significant increases during El Niño and decreases in La Niña. We find statistically significant increases for all RI measures examined in the NA during La Niña and decreases in El Niño (except 30+ kt RI percentage; Figure 3). In the WNP, there are significant reductions in 30+ kt RI storms and events during La Niña, while changes in 50+ kt RI storms are not significant. This is likely due to the pronounced dipole of TC activity that occurs in the WNP. During El Niño, a strong maximum of RI events occurs near 15°N, 150°E. This maximum shifts northwestward during La Niña (Figure 2b).

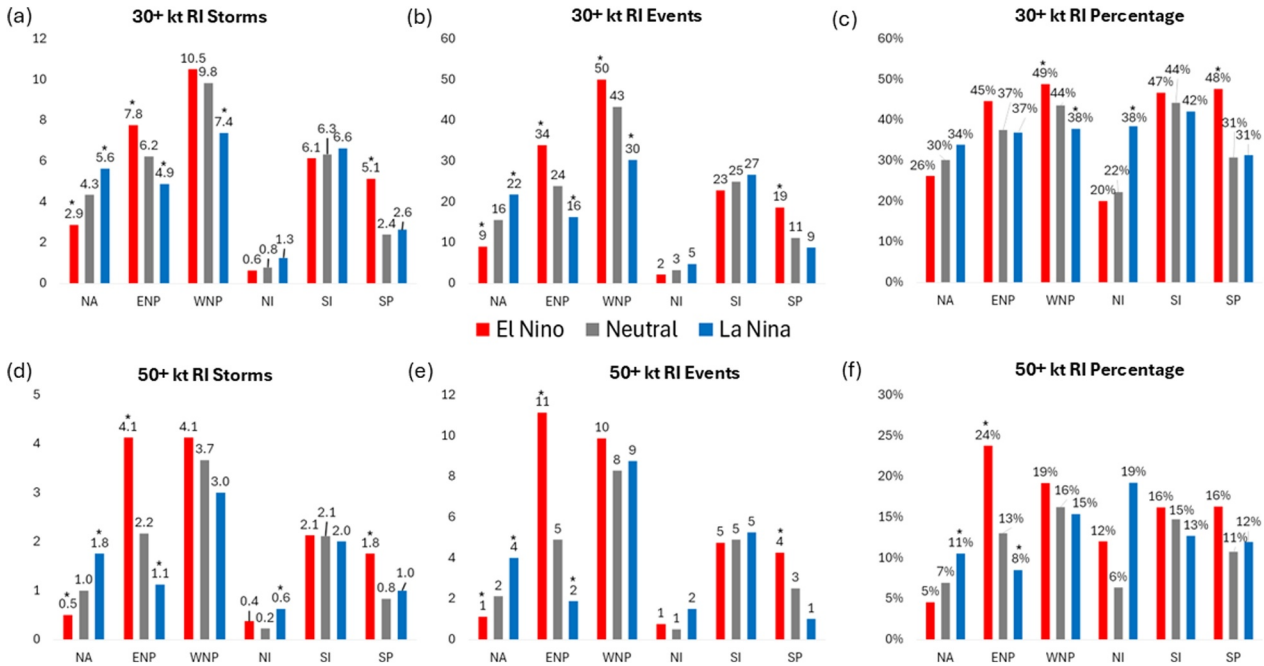

Figure 3. TC basin statistics for the North Atlantic (NA), eastern North Pacific (ENP), western North Pacific (WNP), North Indian (NI), South Indian (SI) and South Pacific (SP) based on ENSO phase. (a, b and c) Average per-year 30 kt RI statistics. (d, e and f) Average per-year 50 kt RI statistics. (a, d) Number of RI storms (b, e) Number of RI events, and (c, f) Percentage of named storms (e.g., maximum sustained winds ≥34 kt) that undergo RI. Note that multiple RI events occur in a typical RI storm. Asterisks denote statistical significance from the 1990–2023 mean at the 10% level.

We do not find significant ENSO-driven modulation of basin wide RI storm activity in the NI or SI basins. In the SI, ENSO-driven environmental modulations produce both favorable and unfavorable conditions for TCs. For example, we find increased shear and increased RH during El Niño in the western part of the basin, while near Australia, environmental conditions are unfavorable for RI, with cooler rSSTs, lower PI, increased shear and decreased RH all contributing to RI suppression. RI events are frequent along the Australian coast (Figure 2), but we do not see a clear modulation of these events by ENSO. In the SP, there are statistically significant increases in all RI metrics (except 50+ kt RI percentage) during El Niño years, driven by more favorable dynamic and thermodynamic conditions (Figures 1d–1f and 3).

The regions with increased RI activity broadly correspond to regions with more TC-favorable conditions (e.g., reduced shear, increased RH and increased PI). While we are looking at averages of large-scale conditions over a several-month period in this analysis, similar to what we find with basinwide seasonal TC forecasts (e.g., Takaya et al., 2022), a shift in the mean towards more TC-favorable large-scale conditions likely increases the chances that a TC will encounter environmental conditions that favor RI.

5. Summary

This study shows a clear relationship, both regionally and basin wide, between TC RI and the phases of ENSO. Our primary results are drawn from observed TCs and observed ENSO events between 1990 and 2023. In the NA, RI occurs more frequently during La Niña than during El Niño, due to reduced wind shear and increased mid-level RH. In the ENP, RI occurs more frequently in El Niño than in La Niña due to increased rSSTs and RH. In the WNP, while RI occurs more frequently in El Niño than in La Niña, large-scale environmental conditions in the basin have more of a dipole-like structure with reduced shear, increased SSTs, PI and RH in the eastern part of the basin and opposite-signed anomalies in the western part of the basin. However, given that TCs forming in the eastern part of the basin tend to have longer tracks over warm SSTs, their odds of undergoing RI are increased. While environmental conditions tend to be more RI-favorable in the NI during La Niña, we do not find significant differences in RI, likely due to the limited sample size of RI events in this basin. In the SP, conditions for RI become more conducive farther east in the basin during El Niño, with increased SSTs, PI and RH and decreased shear all favoring RI. While this study shows that the percentage change of a named storm undergoing RI

10.1029/2025GL115334

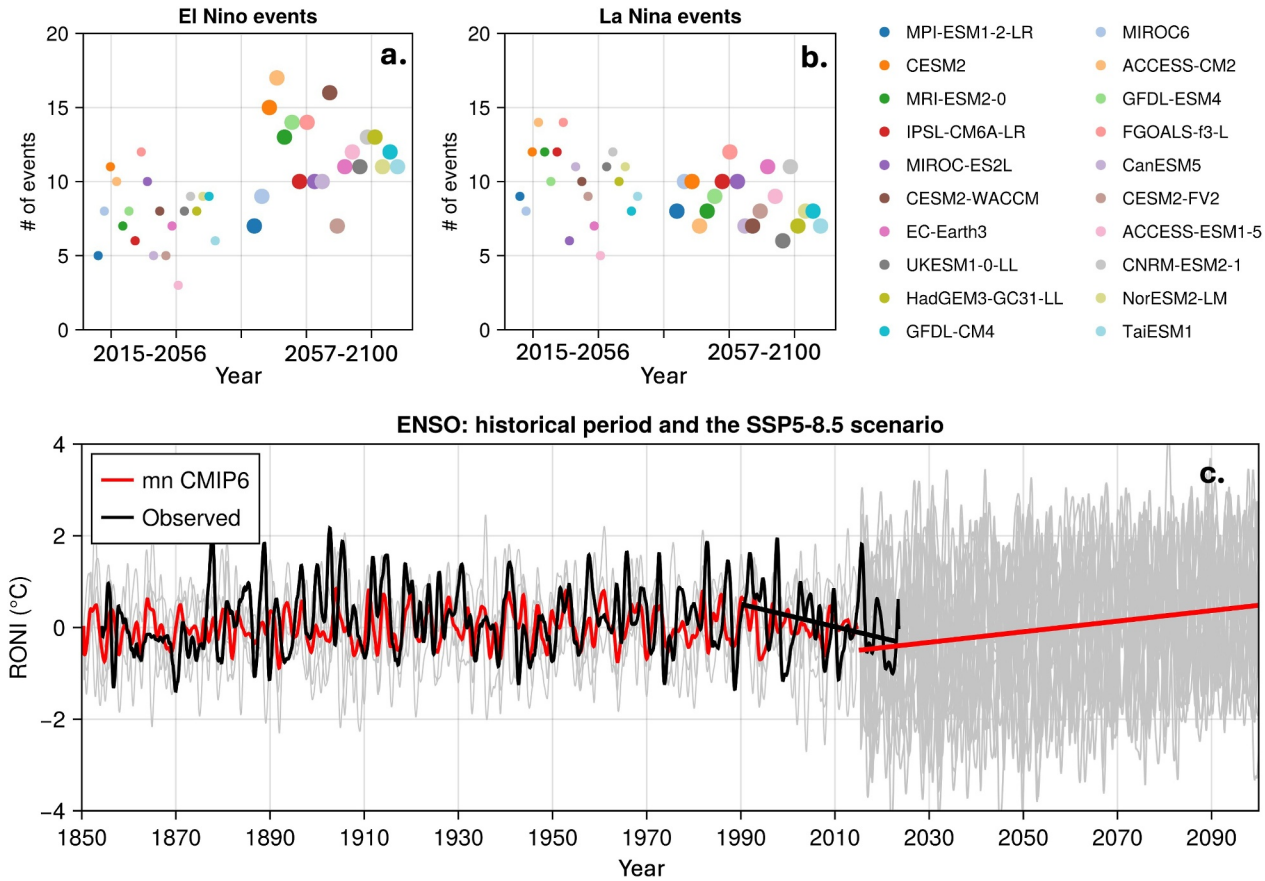

Figure 4. CMIP6 multi-model ENSO analysis. (a, b) Number of events in the SSP5-8.5 scenario between 2015 and 2100 for El Niño and La Niña, respectively, using a RONI threshold of ±1°C. Events from the second half of the scenario are plotted with larger circles. The colors represent individual models as noted in the legend. (c) RONI index for the observed record (black) and CMIP6 models (gray). The multi-model mean timeseries and trend is in red. The data has been smoothed with a 12-month running mean filter for each simulation. Linear trend lines are for the observations (1990–2023; black) and CMIP6 model simulations (2014–2100; red). The multi-model mean trend line (red) is the average of individual trend lines for each of the 20 CMIP6 models.

increased with more TC-favorable environmental conditions, we do not explicitly address how the ratio of RI days to named storm days changed based on ENSO phase. We intend to investigate this in future work. We also note that this study examined 6-month-average environmental conditions. Although RI certainly depends on physical processes that occur on hourly and daily timescales, we hypothesize that these 6-month averages "load the dice" with conditions that either favor or disfavor RI (Figure S1 in Supporting Information S1).

From a disaster management perspective it is important to understand if RI is likely to increase or decrease in the future. Given the connection between RI and ENSO phase, this understanding will depend on the ability of models to correctly simulate ENSO in the future. However, previous studies (e.g., Cai et al., 2021; Erickson & Patricola, 2023; Lee et al., 2022; Sobel et al., 2023), and our multi-model mean analysis, show an increasing occurrence of El Niño events in the future (Figure 4). Based on our current results, the implications for such a scenario would be a general increase of RI in the ENP, the WNP and the SP, along with a decrease in the NA. However, the opposite trend has been occurring in the observational record over the past ∼40 years (e.g., Klotzbach et al., 2022; Lee et al., 2022; Watanabe et al., 2024), with La Niña events tending to occur more frequently towards the end of our study period relative to El Niño events (Table S2 in Supporting Information S1).

Considerable uncertainty remains as to the future characteristics of ENSO, with Watanabe et al. (2024) arguing that El Niño-like states will likely be more common. Additionally, it is not certain that the current relationship between ENSO phase and RI will hold in the future. Our current assumption is that this relationship will continue, but if it does not, the predictive power of ENSO on RI could decrease.

An improved understanding of the discrepancy between the observed La Niña-like trend and the CMIP6-modeled El Niño trend is imperative to better anticipating how RI may change in the future. The predictive power of ENSO for TCs in general, and RI in particular, creates a basis for seasonal hurricane prediction and provides early warnings to communities and response efforts. Clarifying the RI–ENSO relationship will help us to anticipate the possible future impacts of RI.

Conflict of Interest

The authors declare no conflicts of interest relevant to this study.

Data Availability Statement

TC data are from the International Best Track Archive for Climate Stewardship version 4 and is available at Gahtan et al. (2024). ERA5 ECMWF reanalysis data is available at Hersbach et al. (2023). CMIP6 output were downloaded from: https://www.cisl.ucar.edu/computing-data/data/cmip-analysis-platform. PI was calculated using code from: https://github.com/dgilford/tcpyPI.

Acknowledgments
LGS, PK, MMB and SC acknowledge funding from Gallagher Re through the Gallagher Research Centre Global Tropical Cyclone Consortium. LGS, PK, and MMB also acknowledge funding from the Office of Naval Research award N00014-20-1-2069 and the G. Unger Vetlesen Foundation. LGS acknowledges funding from the National Science Foundation award 2327958. We would like to thank Hamish Ramsay, an anonymous reviewer and the editor, Suzana Camargo, for helpful comments that have substantially improved the quality of this manuscript.

References

Astier, N., Plu, M., & Claud, C. (2015). Associations between tropical cyclone activity in the southwest Indian Ocean and El Niño Southern oscillation. *Atmospheric Science Letters*, *16*(4), 506–511. https://doi.org/10.1002/asl.589

Balaguru, K., Patricola, C. M., Hagos, S. M., Leung, L. R., & Dong, L. (2020). Enhanced predictability of eastern North Pacific tropical cyclone activity using the ENSO longitude index. *Geophysical Research Letters*, *47*(16), e2020GL088849. https://doi.org/10.1029/2020GL088849

Bhatia, K. T., Baker, A., Yang, W., Vecchi, G. A., Knutson, T. R., Murakami, H., et al. (2022). A potential explanation for the global increase in tropical cyclone rapid intensification. *Nature Communications*, *13*(1), 6626. https://doi.org/10.1038/s41467-022-34321-6

Bhatia, K. T., Vecchi, G. A., Knutson, T. R., Murakami, H., Kossin, J., Dixon, K. W., & Whitlock, C. E. (2019). Recent increases in tropical cyclone intensification rates. *Nature Communications*, *10*(1), 635. https://doi.org/10.1038/s41467-019-08471-z

Bister, M., & Emanuel, K. A. (2002). Low frequency variability of tropical cyclone potential intensity. 1: Interannual to interdecadal variability. *Journal of Geophysical Research*, *107*(D24), 4801. https://doi.org/10.1029/2001JD000776

Cai, W., Santoso, A., Collins, M., Dewitte, B., Karamperidou, C., Kug, J. S., et al. (2021). Changing El Niño–Southern oscillation in a warming climate. *Nature Reviews Earth & Environment*, *2*(9), 628–644. https://doi.org/10.1038/s43017-021-00199-z

Camargo, S. J., Emanuel, K. A., & Sobel, A. H. (2007). Use of a genesis potential index to diagnose ENSO effects on tropical cyclone genesis. *Journal of Climate*, *20*(19), 4819–4834. https://doi.org/10.1175/JCLI4282.1

Cha, T.-Y., Bell, M. M., Lee, W.-C., & DesRosiers, A. J. (2020). Polygonal eyewall asymmetries during the rapid intensification of Hurricane Michael (2018). *Geophysical Research Letters*, *47*(15), e2020GL087919. https://doi.org/10.1029/2020GL087919

Chand, S. S., Tory, K. J., McBride, J. L., Wheeler, M. C., Dare, R. A., & Walsh, K. J. E. (2013). The different impact of positive-neutral and negative-neutral ENSO regimes on Australian tropical cyclones. *Journal of Climate*, *26*(20), 8008–8016. https://doi.org/10.1175/JCLI-D-12-00769.1

Chu, J.-H., Sampson, C. R., Levine, A. S., & Fukada, E. (2002). *The joint typhoon warning center best-tracks, 1945–2000*. Naval Research Laboratory. Retrieved from https://www.metoc.navy.mil/jtwc/products/best-tracks/tc-bt-report.html

Collins, J. M., Klotzbach, P. J., Maue, R. N., Roache, D. R., Blake, E. S., Paxton, C. H., & Mehta, C. A. (2016). The record-breaking 2015 hurricane season in the eastern North Pacific: An analysis of environmental conditions. *Geophysical Research Letters*, *43*(17), 9217–9224. https://doi.org/10.1002/2016GL070597

Das, D., Chiao, S., Roychoudhury, C., Khan, F., Chaudhuri, S., & Mukherjee, S. (2023). Tropical cyclonic energy variability in North Indian Ocean: Insights from ENSO. *Climate*, *11*(12), 232. https://doi.org/10.3390/cli11120232

DesRosiers, A. J., Bell, M. M., Klotzbach, P. J., Fischer, M. S., & Reasor, P. D. (2023). Observed relationships between tropical cyclone vortex height, intensity, and intensification rate. *Geophysical Research Letters*, *50*(8), e2022GL101877. https://doi.org/10.1029/2022GL101877

Dowdy, A. J. (2014). Long-term changes in Australian tropical cyclone numbers. *Atmospheric Science Letters*, *15*(4), 292–298. https://doi.org/10.1002/asl2.502

Emanuel, K. A. (1986). An air-sea interaction theory for tropical cyclones. Part I: Steady-state maintenance. *Journal of the Atmospheric Sciences*, *43*(6), 585–605. https://doi.org/10.1175/1520-0469(1986)043<0585:aasitf>2.0.co;2

Erickson, N. E., & Patricola, C. M. (2023). Future projections of the El Niño-southern oscillation and tropical Pacific mean state in CMIP6. *Journal of Geophysical Research: Atmospheres*, *128*(21), e2022JD037 563. https://doi.org/10.1029/2022JD037563

Eyring, V., Bony, S., Meehl, G., Senior, C. A., Stevens, B., Stouffer, R. J., & Taylor, K. E. (2016). Overview of the Coupled Model Intercomparison Project Phase 6 (CMIP6) experimental design and organization. *Geoscientific Model Development*, *9*(5), 1937–1958. https://doi.org/10.5194/gmd-9-1937-2016

Gahtan, J., Knapp, K. R., Schreck, C. J., Diamond, H. J., Kossin, J. P., & Kruk, M. C. (2024). International Best Track Archive for Climate Stewardship (IBTrACS) project, version 4r01 [Dataset]. *NOAA National Centers for Environmental Information*. https://doi.org/10.25921/82ty-9e16

Gilford, D. M. (2020). pyPI: Potential intensity calculations in python, v1.3. *Zenodo*. https://doi.org/10.5281/zenodo.3985975

Gilford, D. M. (2021). pyPI (v1.3): Tropical cyclone potential intensity calculations in python. *Geoscientific Model Development*, *14*(5), 2351–2369. https://doi.org/10.5194/gmd-14-2351-2021

Good, P. (2005). *Permutation, parametric and bootstrap tests of hypotheses* (3rd ed.). Springer. https://doi.org/10.1007/b138696

Guo, Y.-P., & Tan, Z.-M. (2021). Influence of different ENSO types on tropical cyclone rapid intensification over the western north Pacific. *Journal of Geophysical Research: Atmospheres*, *126*(11), e2020JD033059. https://doi.org/10.1029/2020JD033059

Hazelton, A. T., Zhang, X., Gopalakrishnan, S., Ramstrom, W., Marks, F., & Zhang, J. A. (2020). High-resolution ensemble HFV3 forecasts of Hurricane Michael (2018): Rapid intensification in shear. *Monthly Weather Review*, *148*(5), 2009–2032. https://doi.org/10.1175/MWR-D-19-0275.1

Hendricks, E. A., Peng, M. S., Fu, B., & Li, T. (2010). Quantifying environmental control on tropical cyclone intensity change. *Monthly Weather Review*, *138*(8), 3243–3271. https://doi.org/10.1175/2010MWR3185.1

Hersbach, H., Bell, B., Berrisford, P., Biavati, G., Horányi, A., Muñoz Sabater, J., et al. (2023). ERA5 monthly averaged data on pressure levels from 1940 to present [Dataset]. *Copernicus Climate Change Service (C3S) Climate Data Store (CDS)*. https://doi.org/10.24381/cds.6860a573

Hersbach, H., Bell, B., Berrisford, P., Hirahara, S., Horanyi, A., Munoz-Sabater, J., et al. (2020). The ERA5 global reanalysis. *Quarterly Journal of the Royal Meteorological Society*, *146*(730), 1999–2049. https://doi.org/10.1002/qj.3803

Ho, C.-H., Kim, J.-H., Jeong, J.-H., Kim, H.-S., & Chen, D. (2006). Variation of tropical cyclone activity in the South Indian Ocean: El Niño–Southern oscillation and Madden-Julian Oscillation effects. *Journal of Geophysical Research*, *111*, D22101. https://doi.org/10.1029/2006JD007289

Huang, B., Thorne, P. W., Banzon, V. F., Boyer, T., Chepurin, G., Lawrimore, J. H., et al. (2017). Extended Reconstructed Sea SurfA Temperature version 5 (ERSSTv5): Upgrades, validations and intercomparisons. *Journal of Climate*, *30*(20), 8179–8205. https://doi.org/10.1029/2006JD007289

Jin, F.-F. (1997). An equatorial ocean recharge paradigm for ENSO. Part 1: Conceptual model. *Journal of the Atmospheric Sciences*, *54*(7), 811–829. https://doi.org/10.1175/1520-0469(1997)054<0811:aeorpf>2.0.co;2

Kaplan, J., & DeMaria, M. (2003). Large-scale characteristics of rapidly intensifying tropical cyclones in the North Atlantic basin. *Weather and Forecasting*, *18*(6), 1093–1108. https://doi.org/10.1175/1520-0434(2003)018<1093:lcorit>2.0.co;2

Klotzbach, P. J. (2011). The influence of El Niño–Southern oscillation and the Atlantic multidecadal oscillation on Caribbean tropical cyclone activity. *Journal of Climate*, *24*(3), 721–731. https://doi.org/10.1175/2010JCLI3705.1

Klotzbach, P. J. (2012). El Niño-Southern oscillation, the Madden-Julian oscillation and Atlantic basin tropical cyclone rapid intensification. *Geophysical Research Letters*, *117*, D14104. https://doi.org/10.1029/2012JD017714

Klotzbach, P. J., & Landsea, C. W. (2015). Extremely intense hurricanes: Revisiting Webster et al. (2005) after 10 years. *Journal of Climate*, *28*(19), 7621–7629. https://doi.org/10.1175/JCLI-D-15-0188.1

Klotzbach, P. J., Wood, K. M., Schreck, C. J., III, Bowen, S. G., Patricola, C. M., & Bell, M. M. (2022). Trends in global tropical cyclone activity: 1990–2021. *Geophysical Research Letters*, *49*(6), e2021GL095774. https://doi.org/10.1029/2021GL095774

Knapp, K. R., Kruk, M. C., Levinson, D. H., Diamond, H. J., & Neumann, C. J. (2010). The International Best Track Archive for Climate Stewardship (IBTrACS). Unifying tropical cyclone data. *Bulletin of the American Meteorological Society*, *91*(3), 363–376. https://doi.org/10.1175/2009BAMS2755.1

Kumar, S., Chand, S., Ramsay, H., Klotzbach, P. J., Courtney, J., Koschatsky, V., & Kumar, S. (2025). An inter-comparison of tropical cyclone datasets for the Australian region. *Environmental Research Letters*, *20*(1), 014039. https://doi.org/10.1088/1748-9326/ad9d5e

Landsea, C. W., & Franklin, J. L. (2013). Atlantic hurricane database uncertainty and presentation of a new database format. *Monthly Weather Review*, *141*(10), 3576–3592. https://doi.org/10.1175/MWR-D-12-00254.1

Lee, S., L'Heureux, M., Wittenberg, A. T., Seager, R., O'Gorman, P. A., & Johnson, N. C. (2022). On the future zonal constraint of equatorial Pacific climate: Perspectives from observations, simulations and theories. *npj Climate and Atmospheric Science*, *5*(82), 82. https://doi.org/10.1038/s41612-022-00301-2

L'Heureux, M. L., Tippett, M. K., Wheeler, M. C., Nguyen, H., Narsey, S., Johnson, N., et al. (2024). A relative sea surface temperature index for classifying ENSO events in a changing climate. *Journal of Climate*, *37*(4), 1197–1211. https://doi.org/10.1175/JCLI-D-23-0406.1

Li, Y., Tang, Y., Wang, S., Toumi, R., Song, X., & Wang, Q. (2023). Recent increases in tropical cyclone rapid intensification events in global offshore regions. *Nature Communications*, *14*(1), 5157. https://doi.org/10.1038/s41467-023-40605-2

Lin, I.-I., Camargo, S. J., Patricola, C. M., Boucharel, J., Chand, S., Klotzbach, P., et al. (2020). ENSO and tropical cyclones. In M. J. McPhaden, A. Santoso, & W. Cai (Eds.), *El Niño southern oscillation in a changing climate*. https://doi.org/10.1002/9781119548164.ch17

Magee, A. D., Lorrey, A. M., Kiem, A. S., & Colyvas, K. (2020). A new island-scale tropical cyclone outlook for southwest Pacific nations and territories. *Scientific Reports*, *10*(1), 11286. https://doi.org/10.1038/s41598-020-67646-7

Majumdar, S. J., Nebylitsa, S., Klotzbach, P. J., Masiello, C., & Michael, Z. R. (2023). North Atlantic tropical cyclone intensification: Regional environmental drivers and trends. *Geophysical Research Letters*, *50*(17), e2023GL104803. https://doi.org/10.1029/2023GL104803

Miyamoto, Y., & Nolan, D. S. (2018). Structural changes preceding rapid intensification in tropical cyclones as shown in a large ensemble of idealized simulations. *Journal of the Atmospheric Sciences*, *75*(2), 555–569. https://doi.org/10.1175/JAS-D-17-0177.1

Mueller, T. J., Patricola, C. M., & Bercos-Hickey, E. (2024). The influence of ENSO diversity on future Atlantic tropical cyclone activity. *Journal of Climate*, *37*(15), 3959–3975. https://doi.org/10.1175/JCLI-D-23-0286.1

Ng, C. H. J., & Vecchi, G. A. (2020). Large-scale environmental controls on the seasonal statistics of rapidly intensifying North Atlantic tropical cyclones. *Climate Dynamics*, *54*(9–10), 3907–3925. https://doi.org/10.1007/s00382-020-05207-4

O'Neill, B. C., Tebaldi, C., van Vuuren, D. P., Eyring, V., Friedlingstein, P., Hurtt, G., et al. (2016). The Scenario Model Intercomparison Project (ScenarioMIP) for CMIP6. *Geoscientific Model Development*, *9*, 3461–3482. https://doi.org/10.5194/gmd-9-3461-2016

Patricola, C. M., Camargo, S. J., Klotzbach, P. J., Saravanan, R., & Chang, P. (2018). The influence of ENSO flavors on western North Pacific tropical cyclone activity. *Journal of Climate*, *31*(14), 5395–5416. https://doi.org/10.1175/JCLI-D-17-0678.1

Patricola, C. M., Cassidy, D. J., & Klotzbach, P. J. (2022). Tropical oceanic influences on observed global tropical cyclone frequency. *Geophysical Research Letters*, *49*(13), e2022GL099354. https://doi.org/10.1029/2022GL099354

Ramsay, H. A., & Sobel, A. H. (2011). Effects of relative and absolute sea surface temperature on tropical cyclone potential intensity using a single-column model. *Journal of Climate*, *24*(1), 183–193. https://doi.org/10.1175/2010jcli3690.1

Rasmusson, E. M., & Carpenter, T. H. (1982). Variations in tropical sea surface temperature and surface wind fields associated with the southern Oscillation/El Niño. *Monthly Weather Review*, *110*(5), 354–384. https://doi.org/10.1175/1520-0493(1982)110<0354:VITSST>2.0.CO;2

Richardson, J. C., Torn, R. D., & Tang, B. H. (2022). An analog comparison between rapidly and slowly intensifying tropical cyclones. *Monthly Weather Review*, *150*(8), 2139–2156. https://doi.org/10.1175/MWR-D-21-0260.1

Roberts, M. J., Camp, J., Seddon, J., Vidale, P. L., Hodges, K., Vannière, B., et al. (2020). Projected future changes in tropical cyclones using the CMIP6 HighResMIP multimodel ensemble. *Geophysical Research Letters*, *47*(14), e2020GL088662. https://doi.org/10.1029/2020GL088662

Roose, S., Ajayamohan, R. S., Ray, P., Mohan, P. R., & Mokanakumar (2022). ENSO influence on Bay of Bengal cyclogenesis confined to low latitudes. *npj Climate and Atmospheric Science*, *5*(1), 31. https://doi.org/10.1038/s41612-022-00252-8

Rozoff, C. M., & Kossin, J. P. (2011). New probabilistic forecast models for the prediction of tropical cyclone rapid intensification. *Weather and Forecasting*, *26*(5), 677–689. https://doi.org/10.1175/WAF-D-10-05059.1

Schreck, C. J., III., Knapp, K. R., & Kossin, J. P. (2014). The impact of best track discrepancies on global tropical cyclone climatologies using IBTrACS. *Monthly Weather Review*, *142*(10), 3881–3899. https://doi.org/10.1175/MWR-D-14-00021.1

Sobel, A. H., Lee, C., Bowen, S. G., Camargo, S. J., Cane, M. A., Clement, A., et al. (2023). Near-term tropical cyclone risk and coupled Earth system model biases. *Proceedings of the National Academy of Sciences*, *120*(33), e2209631120. https://doi.org/10.1073/pnas.2209631120

Stern, D. P., Vigh, J. L., Nolan, D. S., & Zhang, F. (2015). Revisiting the relationship between eyewall contraction and intensification. *Journal of the Atmospheric Sciences*, *72*(4), 1283–1306. https://doi.org/10.1175/JAS-D-14-0261.1

Takaya, Y., Caron, L. P., Blake, E., Bonnardot, F., Bruneau, N., Camp, J., et al. (2022). Recent advances in seasonal and multi-annual tropical cyclone forecasting. *Tropical Cyclone Research and Review*, *12*(3), 182–199. https://doi.org/10.1016/j.tcrr.2023.09.003

Trabing, B. C., & Bell, M. M. (2020). Understanding rapid intensity changes in official hurricane intensity forecast error distributions. *Weather and Forecasting*, *35*(6), 2219–2234. https://doi.org/10.1175/WAF-D-19-0253.1

van Oldenborgh, G. J., Hendon, H., Stockdale, T., L'Heureux, M., de Perez, E. C., Singh, R., & van Aalst, M. (2021). Defining El Niño indices in a warming climate. *Environmental Research Letters*, *16*, 044003. https://doi.org/10.1088/1748-9326/abe9ed

Vecchi, G. A., & Soden, B. J. (2007). Effect of remote sea surface temperature change on tropical cyclone potential intensity. *Nature*, *450*(7172), 1066–1070. https://doi.org/10.1038/nature06423

Wang, C., Wang, X., Weisberg, R. H., & Black, M. L. (2017). Variability of tropical cyclone rapid intensification in the North Atlantic and its relationship with climate variations. *Climate Dynamics*, *49*(11–12), 3627–3645. https://doi.org/10.1007/s00382-017-3537-9

Wang, Z., Zhang, G., Dunkerton, T. J., & Jin, F.-F. (2020). Summertime stationary waves integrate tropical and extratropical impacts on tropical cyclone activity. *Proceedings of the National Academy of Sciences*, *117*(37), 22720–22726. https://doi.org/10.1073/pnas.2010547117

Watanabe, M., Kang, S. M., Collins, M., Hwang, Y.-T., McGregor, S., & Stuecker, M. F. (2024). Possible shifts in controls of the tropical Pacific surface warming pattern. *Nature*, *630*(8016), 315–324. https://doi.org/10.1038/s41586-024-07452-7

Wilks, D. S. (2016). "The stippling shows statistically significant grid points" how research results are routinely overstated and overinterpreted, and what to do about it. *Bulletin of the American Meteorological Society*, *97*(12), 2263–2273. https://doi.org/10.1175/BAMS-D-15-00267.1

Zhao, J., Zhan, R., Murakami, H., Wang, Y., Xie, S.-P., Zhang, L., & Guo, Y. (2023). Atmospheric modes fiddling the simulated ENSO impact on tropical cyclone genesis over the Northwest Pacific. *npj Climate and Atmospheric Science*, *6*(1), 213. https://doi.org/10.1038/s41612-023-00537-6

References From the Supporting Information

Beobide-Arsuaga, G., Bayr, T., Reintges, A., & Latif, M. (2021). Uncertainty of ENSO-amplitude projections in CMIP5 and CMIP6 models. *Climate Dynamics*, *56*(11–12), 3875–3888. https://doi.org/10.1007/s00382-021-05673-4

Boucher, O., Denvil, S., Levavasseur, G., Cozic, A., Caubel, A., Foujols, M.-A., et al. (2019). *IPSL IPSL-CM6A-LR model output prepared for CMIP6 ScenarioMIP ssp585*. Earth System Grid Federation. https://doi.org/10.22033/ESGF/CMIP6.5271

Brovkin, V., Wieners, K.-H., Giorgetta, M., Jungclaus, J., Reick, C., Esch, M., et al. (2019). MPI-M MPI-ESM1.2-LR model output prepared for CMIP6 C4MIP esm-ssp585. *Earth System Grid Federation*. https://doi.org/10.22033/ESGF/CMIP6.6558

Danabasoglu, G. (2019a). NCAR CESM2 model output prepared for CMIP6 C4MIP esm-ssp585. *Earth System Grid Federation*. https://doi.org/10.22033/ESGF/CMIP6.7582

Danabasoglu, G. (2019b). NCAR CESM2-WACCM model output prepared for CMIP6 ScenarioMIP ssp585. *Earth System Grid Federation*. https://doi.org/10.22033/ESGF/CMIP6.10115

Dix, M., Bi, D., Dobrohotoff, P., Fiedler, R., Harman, I., Law, R., et al. (2019). CSIRO-ARCCSS ACCESS-CM2 model output prepared for CMIP6 ScenarioMIP ssp585. *Earth System Grid Federation*. https://doi.org/10.22033/ESGF/CMIP6.4332

EC-Earth Consortium (EC-Earth). (2021). EC-Earth-Consortium EC-Earth-3-CC model output prepared for CMIP6 C4MIP esm-ssp585. *Earth System Grid Federation*. https://doi.org/10.22033/ESGF/CMIP6.4650

Good, P. (2020). MOHC HadGEM3-GC31-LL model output prepared for CMIP6 ScenarioMIP ssp585. *Earth System Grid Federation*. https://doi.org/10.22033/ESGF/CMIP6.10901

Guo, H., John, J., Blanton, C., McHugh, C., Nikonov, S., Radhakrishnan, A., et al. (2018). NOAA-GFDL GFDL-CM4 model output prepared for CMIP6 ScenarioMIP ssp585. *Earth System Grid Federation*. https://doi.org/10.22033/ESGF/CMIP6.9268

Hajima, T., Kawamiya, M., Tachiiri, K., Abe, M., Arakawa, O., Suzuki, T., et al. (2020). MIROC MIROC-ES2L model output prepared for CMIP6 C4MIP esm-ssp585. *Earth System Grid Federation*. https://doi.org/10.22033/ESGF/CMIP6.5526

Jones, C. (2019). MOHC UKESM1.0-LL model output prepared for CMIP6 C4MIP esm-ssp585. *Earth System Grid Federation*. https://doi.org/10.22033/ESGF/CMIP6.5969

Krasting, J. P., Blanton, C., McHugh, C., Radhakrishnan, A., John, J. G., Rand, K., et al. (2018). NOAA-GFDL GFDL-ESM4 model output prepared for CMIP6 C4MIP esm-ssp585. *Earth System Grid Federation*. https://doi.org/10.22033/ESGF/CMIP6.8545

Lee, W.-L., & Liang, H.-C. (2020). *AS-RCEC TaiESM1.0 model output prepared for CMIP6 CMIP abrupt-4xCO2*. Earth System Grid Federation. https://doi.org/10.22033/ESGF/CMIP6.9709

Magee, A. D., Verdon-Kidd, D. C., Diamond, H. J., & Kiem, A. S. (2017). Influence of ENSO, ENSO Modoki, and the IPO on tropical cyclogenesis: A spatial analysis of the southwest Pacific region. *International Journal of Climatology*, *37*(S1), 1118–1137. https://doi.org/10.1002/joc.5070

National Center for Atmospheric Research (NCAR). (2022). NCAR CESM2-FV2 model output prepared for CMIP6 ScenarioMIP ssp585. *Earth System Grid Federation*. https://doi.org/10.22033/ESGF/CMIP6.17669

Schwinger, J., Tjiputra, J., Seland, Ø., Bentsen, M., Oliviè, D. J. L., Toniazzo, T., et al. (2020). NCC NorESM2-LM model output prepared for CMIP6 C4MIP esm-ssp585. *Earth System Grid Federation*. https://doi.org/10.22033/ESGF/CMIP6.13748

Seferian, R. (2020). CNRM-CERFACS CNRM-ESM2-1 model output prepared for CMIP6 C4MIP esm-ssp585. *Earth System Grid Federation*. https://doi.org/10.22033/ESGF/CMIP6.4017

Shiogama, H., Abe, M., & Tatebe, H. (2019). MIROC MIROC6 model output prepared for CMIP6 ScenarioMIP ssp585. *Earth System Grid Federation*. https://doi.org/10.22033/ESGF/CMIP6.5771

Swart, N. C., Cole, J. N. S., Kharin, V. V., Lazare, M., Scinocca, J. F., Gillett, N. P., et al. (2019). CCCma CanESM5-CanOE model output prepared for CMIP6 C4MIP esm-ssp585. *Earth System Grid Federation*. https://doi.org/10.22033/ESGF/CMIP6.10242

Yu, Y. (2019). CAS FGOALS-f3-L model output prepared for CMIP6 ScenarioMIP ssp585. *Earth System Grid Federation*. https://doi.org/10.22033/ESGF/CMIP6.3502

Yukimoto, S., Koshiro, T., Kawai, H., Oshima, N., Yoshida, K., Urakawa, S., et al. (2019). MRI MRI-ESM2.0 model output prepared for CMIP6 C4MIP esm-ssp585. *Earth System Grid Federation*. https://doi.org/10.22033/ESGF/CMIP6.6811

Ziehn, T., Chamberlain, M., Lenton, A., Law, R., Bodman, R., Dix, M., et al. (2019). CSIRO ACCESS-ESM1.5 model output prepared for CMIP6 C4MIP esm-ssp585. *Earth System Grid Federation*. https://doi.org/10.22033/ESGF/CMIP6.4252